Osteoporosis International (2018) 29:2685–2692
https://doi.org/10.1007/s00198-018-4675-6

ORIGINAL ARTICLE

Effects of virtual tube current reduction and sparse sampling on MDCT-based femoral BMD measurements

N. Sollmann[1,2] · K. Mei[3] · B.J. Schwaiger[3] · A.S. Gersing[3] · F.K. Kopp[3] · R. Bippus[4] · C. Maegerlein[1] · C. Zimmer[1] · E.J. Rummeny[3] · J.S. Kirschke[1] · P.B. Noël[3] · T. Baum[1]

Received: 30 January 2018 / Accepted: 14 August 2018 / Published online: 24 August 2018

Abstract

Summary This study investigates the impact of tube current reduction and sparse sampling on femoral bone mineral density (BMD) measurements derived from multi-detector computed tomography (MDCT). The application of sparse sampling led to robust and clinically acceptable BMD measurements. In contrast, BMD measurements derived from MDCT with virtually reduced tube currents showed a considerable increase when compared to original data.

Introduction The study aims to evaluate the effects of radiation dose reduction by using virtual reduction of tube current or sparse sampling combined with standard filtered back projection (FBP) and statistical iterative reconstruction (SIR) on femoral bone mineral density (BMD) measurements derived from multi-detector computed tomography (MDCT).

Methods In routine MDCT scans of 41 subjects (65.9% men; age 69.3 ± 10.1 years), reduced radiation doses were simulated by lowering tube currents and applying sparse sampling (50, 25, and 10% of the original tube current and projections, respectively). Images were reconstructed using FBP and SIR. BMD values were assessed in the femoral neck and compared between the different dose levels, numbers of projections, and image reconstruction approaches.

Results Compared to full-dose MDCT, virtual lowering of the tube current by applying our simulation algorithm resulted in increases in BMD values for both FBP (up to a relative change of 32.5%) and SIR (up to a relative change of 32.3%). In contrast, the application of sparse sampling with a reduction down to 10% of projections showed robust BMD values, with clinically acceptable relative changes of up to 0.5% (FBP) and 0.7% (SIR).

N. Sollmann and K. Mei contributed equally to this work.

Ethics Committee Registration Number: 5022/11-A1

✉ N. Sollmann
Nico.Sollmann@tum.de

K. Mei
Kai.Mei@tum.de

B.J. Schwaiger
Benedikt.Schwaiger@tum.de

A.S. Gersing
Alexandra.Gersing@tum.de

F.K. Kopp
Felix.Kopp@tum.de

R. Bippus
Rolf.Bippus@philips.com

C. Maegerlein
Christian.Maegerlein@tum.de

C. Zimmer
Claus.Zimmer@tum.de

E.J. Rummeny
Ernst.Rummeny@tum.de

J.S. Kirschke
Jan.Kirschke@tum.de

P.B. Noël
Peter.Noel@tum.de

T. Baum
Thomas.Baum@tum.de

[1] Department of Diagnostic and Interventional Neuroradiology, Klinikum rechts der Isar, Technische Universität München, Ismaninger Str. 22, 81675 Munich, Germany

[2] TUM-Neuroimaging Center, Klinikum rechts der Isar, Technische Universität München, Munich, Germany

[3] Department of Diagnostic and Interventional Radiology, Klinikum rechts der Isar, Technische Universität München, Ismaninger Str. 22, 81675 Munich, Germany

[4] Philips GmbH Innovative Technologies, Research Laboratories, Röntgenstr. 24-26, 22335 Hamburg, Germany

Conclusions Our simulations, which still require clinical validation, indicate that reductions down to ultra-low tube currents have a significant impact on MDCT-based femoral BMD measurements. In contrast, the application of sparse-sampled MDCT seems a promising future clinical option that may enable a significant reduction of the radiation dose without considerable changes of BMD values.

Keywords Bone mineral density · Computed tomography · Femur · Filtered back projection · Sparse sampling · Statistical iterative reconstruction

Introduction

Osteoporosis is characterized by low bone mass in combination with a micro-architectural deterioration of bone tissue [1]. Since the late 1980s, dual-energy X-ray absorptiometry (DXA) represents the clinical standard method for quantitative imaging in osteoporosis, which enables measurements of bone mineral density (BMD), most commonly applied at the lumbar spine and/or proximal femur [2–5]. The diagnosis of osteoporosis is then based on DXA-derived T-scores [4, 5]. However, despite its high clinical relevance, DXA also has its shortcomings because it has demonstrated to be partly insufficient in identifying subjects at high risk for fractures, which represents a major complication of osteoporosis. In this context, previous studies have shown that over 50% of non-vertebral fractures occurred in patients who showed non-pathological BMD values according to DXA [6, 7].

Recently, volumetric BMD measurements, assessed using multi-detector computed tomography (MDCT), have shown to be feasible particularly at the spine, but also at the femur [8–11]. However, broad clinical use of MDCT-based BMD measurements is currently restricted due to the fairly high radiation doses, which are especially relevant if multiple measurements are required due to reevaluation purposes or therapy monitoring [12]. Consequently, a reduction of the radiation dose for MDCT-based BMD measurements seems necessary.

Amongst various options, a reduction of the radiation dose can be achieved by lowering the tube current or by acquiring fewer projections during scanning, commonly referred to as sparse sampling [13–15]. However, decreased tube current and sparse sampling usually come at the cost of a decrease in image quality, which may limit the validity and clinical usefulness of the examination [13–15]. Constrained image quality, however, can be partially compensated for by applying advanced reconstruction algorithms, such as statistical iterative reconstruction (SIR). In contrast to standard reconstruction methods, like the widely used filtered back projection (FBP), SIR is capable of integrating a physics model, thus having the potential to provide increased image quality when compared to FBP in terms of missing data or lowered tube current during the scan [16–18]. Iterative-based reconstruction approaches use regularization terms to resolve image noise and streaking artifacts, consequently resulting in smoother images [16–18]. Furthermore, such approaches have already been successfully applied in studies using reduced tube current or fewer projections during a scan [19–22].

The purpose of this study was to systematically evaluate the effects of virtual tube current reduction and sparse sampling on MDCT-based BMD measurements at the femoral neck. In this context, we applied both FBP and SIR for image reconstructions and compared BMD values derived from virtual low-dose and sparse-sampled MDCT to original full-dose imaging data.

Methods

Subjects

This study was approved by the local institutional review board (registration number 5022/11-A1). Subjects older than 50 years of age who had undergone a routine thoracic and abdominal MDCT in the clinical setting were retrospectively identified in our institutional digital Picture Archiving and Communication System (PACS). All MDCT scans were performed for clinical purposes. Exclusion criteria were any history of malignant bone lesions (e.g., bone metastases), hematological disorders, any history of a proximal femur fracture, implantation of hip endoprotheses, and metabolic bone disorders aside from osteoporosis. Overall, 41 subjects (14 women and 27 men; age 69.3 ± 10.1 years) were included. The field of view of the scans covered the proximal femur of both sides down to the minor trochanter in all subjects.

Multi-detector computed tomography

The scans were acquired using a 256-row MDCT scanner (iCT; Philips Healthcare, Best, The Netherlands). A standard reference phantom (Mindways Osteoporosis Phantom; Austin, TX, USA) was placed in the scanner beneath the subjects for calibration purposes. Tube voltage and rotation time were 120 kVp and 0.4 s in all cases. The pitch ranged from 0.59 to 0.91, and the maximum tube current ranged from 200 to 400 mA, with the exact tube current being implicitly modulated by the scanner. As a result, for the femoral neck, the tube current was approximately 100 to 200 mA. Examinations were performed after the administration of intravenous contrast agent (Imeron 400; Bracco, Konstanz, Germany) using a

high-pressure injector (Fresenius Pilot C; Fresenius Kabi, Bad Homburg, Germany). Intravenous contrast agent injection was performed with a delay of 70 s, a flow rate of 3 mL/s, and a body weight-dependent dose (80 mL for patients with a body weight under 80 kg, 90 mL for patients with a body weight ranging from 80 to 100 kg, 100 mL for patients with a body weight over 100 kg). Additionally, all subjects were given 1000 mL of oral contrast agent over a period of 1 h (Barilux Scan; Sanochemia Diagnostics, Neuss, Germany).

Tube current simulation and sparse sampling

The simulation algorithm to generate lower tube currents for MDCT scans was based on raw projection data, as described previously [13, 23, 24]. System parameters of the MDCT scanner were known to take the electronic noise into account. Low-dose simulations at 50% (D50 P100), 25% (D25 P100), and 10% (D10 P100) of the original tube current were generated. Sparse sampling was applied at levels of 50% (D100 P50), 25% (D100 P25), and 10% (D100 P10) of the original projection data by reading every second, fourth, and tenth projection angle and deleting the remaining projections in the sinogram. Thus, the number of projections per full rotation was reduced, while other parameters, including projection geometry and subject location, were kept the same [13].

Filtered back projection and statistical iterative reconstruction

Images were reconstructed with FBP and SIR [25, 26]. FBP consisted of one step of high-pass filtering (Ram-Lak) in the sinogram domain and another step of normalized three-dimensional cone-beam back-projection [27]. SIR was performed with ordered-subset separable paraboloidal surrogation and a momentum-based accelerating approach [28]. To optimize the image quality for scans with simulated ultra-low doses, a proper regularization was used in SIR [25, 29, 30]. All reconstructions had a voxel spacing of 0.39, 0.39, and 0.30 mm in three dimensions. The actual voxel resolution was limited to the fixed collimator width of the detector. To reduce noise, adjacent axial slices were merged to a slice thickness of 5 mm. Voxel intensities (mass attenuation coefficients, m^2/kg) were calibrated to Hounsfield units (HU) using the mass attenuation coefficient of water.

Measurements of bone mineral density

To derive BMD measurements from original as well as virtual low-dose and sparse-sampled MDCT scans with FBP or SIR, regions of interest (ROIs) were placed in the femoral neck of the left and right sides of each subject. First, axial images of the dataset with 100% of the tube current and 100% of the projections (D100 P100), using FBP as the clinical standard of reference, were opened using ImageJ (https://imagej.nih.gov/ij/) [31, 32]. Then, we identified the axial slice in which the neck was visualized best and drew a quadrangular ROI in this section, including the cortical and trabecular bone compartments (Fig. 1). The same placement strategy and shape of the ROI have been used in a previous study of our group [9]. The two ROIs (femoral neck of both sides) were saved for each subject, and the individual ROIs in the used image stack (D100 P100 with FBP) were then transferred (as intrinsically co-registered) to the other datasets containing the virtual low-dose (D50 P100, D25 P100, and D10 P100) and sparse-sampled imaging data (D100 P50, D100 P25, and D100 P10) of the respective subject, considering both FBP and SIR. We then extracted mean HU from these ROIs, which were subsequently converted into volumetric BMD values (in g/cm^3) using the information of the reference phantom [9, 13]. The BMD values of the left and right sides were averaged in each subject.

Statistical analyses

Statistical data analyses were performed using GraphPad Prism (version 6.04; GraphPad Software, La Jolla, CA, USA). For all statistical tests applied, a p value < 0.05 was considered statistically significant.

Descriptive statistics for BMD values were calculated, including mean, standard deviation, median, minimum, and maximum values. This was done separately for the original imaging data, virtual low-dose, and sparse-sampled MDCT scans in combination with the two different reconstruction

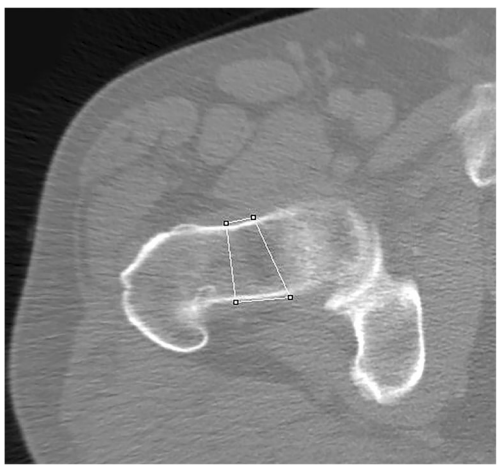

Fig. 1 Placement of regions of interest (ROIs). This figure illustrates the placement of a ROI in the femoral neck in a representative case using axial slices derived from full-dose multi-detector computed tomography (MDCT) using filtered back projection (FBP). The ROI was quadrangular and included the cortex. ROIs were not placed in areas with circumscribed lucencies (e.g., cystic lesions) or sclerosis (e.g., bone islands). The placement of the ROI at the other side's femoral neck was conducted in an analogous way

algorithms. Shapiro-Wilk tests indicated a normal distribution of the obtained BMD values.

In order to evaluate the differences in BMD values derived from MDCT with virtually lowered tube currents and sparse sampling between FBP and SIR, we used paired *t* tests. Furthermore, to assess the change in measurements depending on the tube current and sparse sampling, we compared the BMD values between full-dose MDCT with 100% of the projections (D100 P100) and each value of virtual low-dose (D50 P100, D25 P100, and D10 P100) and sparse-sampled MDCT (D100 P50, D100 P25, and D100 P10) to be able to provide numbers on relative changes. This was performed separately for both reconstructions, FBP and SIR. The BMD measurements were illustrated using box plots.

Results

Virtual lowering of tube currents and sparse sampling using FBP (Fig. 2a) and SIR (Fig. 2b) were successfully achieved in all enrolled subjects. The effective dose of the original scans was estimated to range between 3.6 and 9.1 mSv with a scanning length of 30 cm. BMD measurements for full-dose data using FBP, considered as the current clinical standard, were 0.849 ± 0.106 g/cm^3 (range 0.640–1.060 g/cm^3) in the femoral neck (Table 1).

FBP- and SIR-based BMD values showed an increase with a virtual lowering of the tube current up to 1.125 ± 0.175 g/cm^3 for FBP (D10 P100) and 1.130 ± 0.175 g/cm^3 for SIR (D10 P100), respectively (Table 1 and Fig. 3a, b). Thus, the values for virtual lowering of tube currents showed relative changes up to 32.5% (FBP) and 32.3% (SIR).

Regarding sparse-sampled data, BMD measurements remained comparatively stable in the course of reductions in the number of projections, which was true for both MDCT with FBP and SIR (Table 1 and Fig. 3a, b). Hence, the changes of BMD values regarding sparse-sampled data were clinically acceptable, with small relative changes of up to 0.5% (FBP) and 0.7% (SIR), respectively.

Discussion

This in-vivo study systematically compared the effects of virtual tube current reductions and sparse sampling on MDCT-based femoral BMD measurements using both FBP and SIR. We observed an increase in BMD values with a simulated lowering of the tube current. In contrast, changes in FBP-based and SIR-based BMD values for sparse-sampled data with projections down to 10% of the original data were considerably small.

Due to the small changes of BMD values in the course of reducing the number of projections, BMD measurements

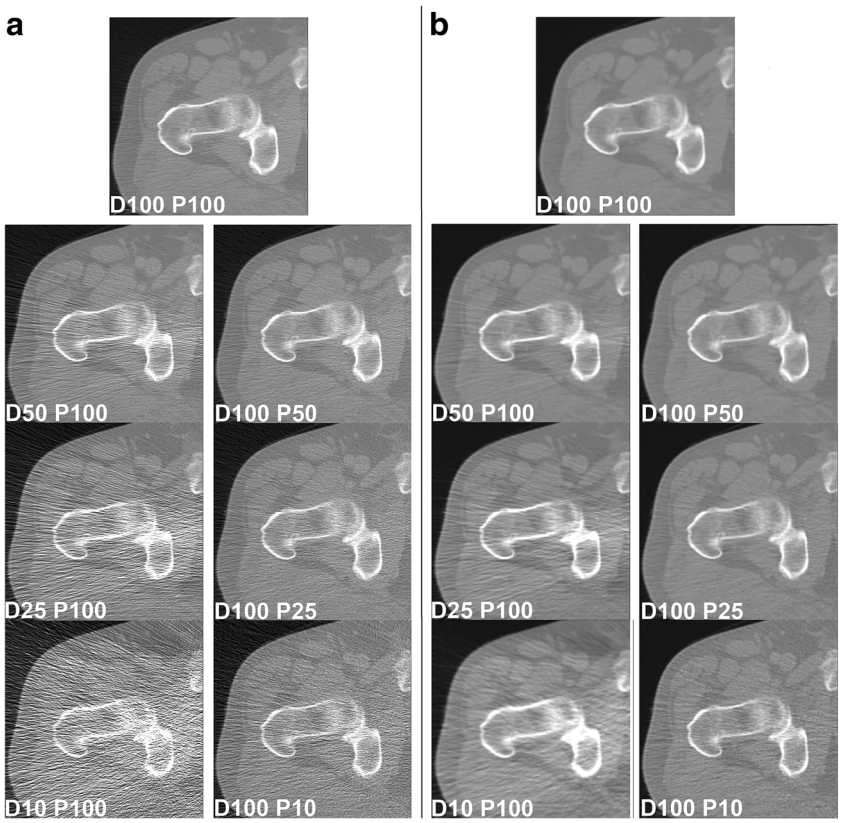

Fig. 2 Low-dose and sparse-sampled multi-detector computed tomography (MDCT). This figure shows axial slices of the femoral neck derived from full-dose MDCT (D100 P100) as well as MDCT at 50% (D50), 25% (D25), and 10% (D10) of the original tube current applied (100% tube current = D100). Furthermore, sparse sampling was performed to achieve 50% (P50), 25% (P25), and 10% (P10) of the original projection data (100% projections = P100). For all settings presented in this figure, filtered back projection (FBP; **a**) and statistical iterative reconstruction (SIR; **b**) were used for image reconstructions

Table 1 Measurements of bone mineral density (BMD)

BMD			D100 P100	D50 P100	D25 P100	D10 P100	D100 P50	D100 P25	D100 P10
Femoral neck	FBP	BMD (g/cm^3; mean ± SD)	0.849 ± 0.106	0.868 ± 0.117	0.928 ± 0.142	1.125 ± 0.175	0.854 ± 0.105	0.860 ± 0.114	0.853 ± 0.106
	SIR	BMD (g/cm^3; mean ± SD)	0.854 ± 0.105	0.875 ± 0.114	0.937 ± 0.141	1.130 ± 0.175	0.861 ± 0.106	0.862 ± 0.106	0.860 ± 0.105
		p value	0.3412	0.2539	0.1151	0.4496	0.2022	0.8296	0.2790

This table shows BMD measurements derived from the femoral neck using filtered back projection (FBP) and statistical iterative reconstruction (SIR). All measurements were performed for full-dose multi-detector computed tomography (MDCT; 100% dose = D100, 100% projections = P100), MDCT with virtually lowered tube currents in relation to original data (50% = D50, 25% = D25, 10% = D10), and MDCT with reduced projections (50% = P50, 25% = P25, 10% = P10). BMD values are given as mean ± standard deviation, and *p* values are derived from comparing BMD values between MDCT with FBP and MDCT with SIR

could be assessed with lower radiation exposure in the future for the femoral neck, an option that has recently been suggested for BMD assessments at the spine [13]. This is a relevant finding for clinical scans since sparse sampling may allow the usage of MDCT for longitudinal risk evaluation and therapy monitoring in subjects with osteoporosis in the future, which is currently restricted due to the high radiation doses of conventional full-dose MDCT without sparse sampling. Because DXA-based BMD measurements are increasingly considered to be non-optimal regarding the reliable identification of subjects at high risk for osteoporotic fractures, broader use of MDCT combined with approaches to reduce radiation exposure seems highly desirable [6, 7]. However, commercially available MDCT scanners are not yet capable of applying sparse sampling to lower radiation exposure since current systems still broadly use X-ray sources that continuously deliver X-rays during the scan. Future systems may implement precise units to individually adjust the number of projections [33].

In contrast, reductions of tube current can easily be achieved nowadays with conventional MDCT scanners. However, BMD measurements clearly increased with virtually decreasing tube currents as compared to original full-dose MDCT data in this study. Current MDCT detectors, such as integrated detectors, have shown that noise will increase when there are not statistically enough X-ray photons reaching the detector [34]. This leads to signal impairment, thus influencing the extraction of BMD values negatively. Therefore, considerable changes in BMD measurements with simulated tube current reductions have occurred according to our analyses. In this context, the noise-related BMD increase observed in our investigations can be difficult to understand. According to theory, the mean value of a given ROI does not depend on noise. A change of values may be related to a change of the energy spectrum reaching the detector or perhaps to non-linearity of the detector. Thus, the results of the simulations may not be observed in clinical practice or to a lower degree. A validation experiment with actual MDCT scans using cadaveric femurs, for example, must be performed before the results can be generalized.

Furthermore, we applied SIR in this study, which is increasingly regarded superior to traditional reconstruction algorithms such as FBP [16–18]. In general, SIR is considered to be more suitable in handling streaking artifacts and noise due to an integration of physics modeling that enables better compensation for missing data, among others [16–18]. Despite the finding that SIR did not yield more robust measurements of BMD values, it is suggested that it can provide enhanced image quality when compared to FBP. However, in this study, we observed that SIR alone is not enough to mitigate the effects of electronic noise caused by ultra-low tube currents at the detector concerning BMD measurements. Future studies will have to further explore settings in which

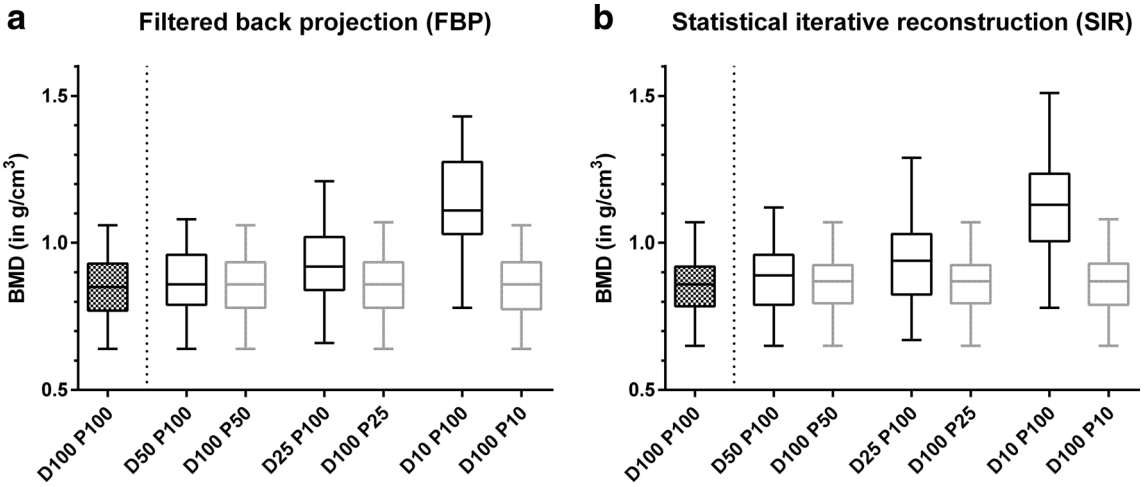

Fig. 3 Measurements of bone mineral density (BMD). This figure shows box plots (with minimum and maximum whiskers) depicting BMD measurements. Values are shown for filtered back-projection (FBP; **a**) and statistical iterative reconstruction (SIR; **b**). All measurements were performed for full-dose multi-detector computed tomography (MDCT; 100% dose = D100, 100% projections = P100), MDCT with virtually lowered tube currents in relation to original data (50% = D50, 25% = D25, 10% = D10), and MDCT with reduced projections when compared to original data (50% = P50, 25% = P25, 10% = P10)

investigators can take the most advantage of SIR that also justifies the related higher computational complexity and power needed.

With regard to the clinical setting, DXA and not MDCT reflects the current standard for quantitative imaging in osteoporosis [2–5]. However, due to shortcomings of DXA, MDCT and other methods are increasingly investigated for BMD measurements [8–11]. Mainly thoracic and abdominal MDCT scans are among the most frequently performed clinical investigations, and applications of such clinical scans for valid BMD measurements, in addition to the primary clinical indication, may reduce the need for DXA, which is often additively performed only for the purpose of BMD measurements. Especially patients who have cancer commonly need assessments of BMD in the course of their disease and treatment because of an increased risk of osteoporosis due to hormone therapy or chemotherapy [35–38]. Thus, this patient cohort could particularly profit from BMD measurements derived from routine MDCT. However, MDCT currently cannot replace DXA when it comes to the diagnosis of osteoporosis since this is still based on DXA-derived T-scores [4, 5].

There are limitations to this study that need to be taken into account. First, this study was designed to be retrospective; thus, our results should be confirmed by future prospective trials. Second, we used routine low-dose MDCT scans and no dedicated quantitative exams. Third, this study only provides BMD values derived from measurements in the femoral neck, thus not representing information about the complete proximal femur. Lastly, MDCT scans were performed with the application of intravenous contrast agent. This effect has to be accounted for to be able to derive valid BMD measurements. However, routine thoracic and abdominal MDCT scans, as used in the present study, are frequently performed after administration of contrast agents, which is especially true in terms of cancer patients who may particularly profit from additional usage of MDCT for BMD assessments as outlined above.

Conclusions

In contrast to virtual tube current reduction, sparse sampling allows for a robust assessment of femoral BMD, even when projection numbers are reduced by 90% of the original data. Thus, the application of sparse-sampled MDCT seems a promising future clinical option that may enable considerable reductions of radiation doses without suffering from clinically relevant changes of BMD values when compared to full-dose MDCT with 100% projections.

Acknowledgements We acknowledge support through the German Department of Education and Research (BMBF) under grant IMEDO (13GW0072C) and the German Research Foundation (DFG) within the Research Training Group GRK 2274.

Funding This project has received funding from the European Research Council (ERC) under the European Union's Horizon 2020 research and innovation program (grant agreement no. 637164—iBack—ERC-2014-STG) and the Nivida Corporation. We furthermore acknowledge support through the German Department of Education and Research (BMBF) under grant IMEDO (13GW0072C).

Compliance with ethical standards

Conflicts of interest Nico Sollmann, Kai Mei, Benedikt J. Schwaiger, Alexandra S. Gersing, Felix K. Kopp, Christian Maegerlein, Claus

Zimmer, Ernst J. Rummeny, Jan S. Kirschke, Peter B. Noël, and Thomas Baum declare that they have no conflict of interest regarding the methods used or results presented in this study. Rolf Bippus is an employee of Philips GmbH Innovative Technologies.

Ethical approval All procedures performed in studies involving human participants were in accordance with the ethical standards of the institutional and with the 1964 Helsinki declaration and its later amendments or comparable ethical standards.

Abbreviations *BMD*, Bone mineral density; *DXA*, Dual-energy X-ray absorptiometry; *FBP*, Filtered back projection; *HU*, Hounsfield units; *MDCT*, Multi-detector computed tomography; *PACS*, Picture Archiving and Communication System; *ROI*, Region of interest; *SIR*, Statistical iterative reconstruction

References

1. NIH Consensus Development Panel on Osteoporosis Prevention Diagnosis and Therapy (2001) Osteoporosis prevention, diagnosis, and therapy. Jama 285:785–795
2. Oei L, Koromani F, Rivadeneira F, Zillikens MC, Oei EH (2016) Quantitative imaging methods in osteoporosis. Quant Imaging Med Surg 6:680–698
3. El Maghraoui A, Roux C (2008) DXA scanning in clinical practice. QJM 101:605–617
4. Lewiecki EM, Binkley N, Morgan SL, Shuhart CR, Camargos BM, Carey JJ, Gordon CM, Jankowski LG, Lee JK, Leslie WD, International Society for Clinical Densitometry (2016) Best practices for dual-energy X-ray absorptiometry measurement and reporting: International Society for Clinical Densitometry Guidance. J Clin Densitom 19:127–140
5. Lewiecki EM, Binkley N, Bilezikian JP, Kendler DL, Leib ES, Petak SM (2006) Official positions of the International Society for Clinical Densitometry. Osteoporos Int 17:1700–1701
6. Schuit SC, van der Klift M, Weel AE, de Laet CE, Burger H, Seeman E, Hofman A, Uitterlinden AG, van Leeuwen JP, Pols HA (2004) Fracture incidence and association with bone mineral density in elderly men and women: the Rotterdam study. Bone 34: 195–202
7. Siris ES, Chen YT, Abbott TA, Barrett-Connor E, Miller PD, Wehren LE, Berger ML (2004) Bone mineral density thresholds for pharmacological intervention to prevent fractures. Arch Intern Med 164:1108–1112
8. Adams JE (2009) Quantitative computed tomography. Eur J Radiol 71:415–424
9. Gruber M, Bauer JS, Dobritz M, Beer AJ, Wolf P, Woertler K, Rummeny EJ, Baum T (2013) Bone mineral density measurements of the proximal femur from routine contrast-enhanced MDCT data sets correlate with dual-energy X-ray absorptiometry. Eur Radiol 23:505–512
10. Bauer JS, Henning TD, Mueller D, Lu Y, Majumdar S, Link TM (2007) Volumetric quantitative CT of the spine and hip derived from contrast-enhanced MDCT: conversion factors. AJR Am J Roentgenol 188:1294–1301
11. Baum T, Muller D, Dobritz M, Rummeny EJ, Link TM, Bauer JS (2011) BMD measurements of the spine derived from sagittal reformations of contrast-enhanced MDCT without dedicated software. Eur J Radiol 80:e140–e145
12. Baum T, Karampinos DC, Liebl H, Rummeny EJ, Waldt S, Bauer JS (2013) High-resolution bone imaging for osteoporosis diagnostics and therapy monitoring using clinical MDCT and MRI. Curr Med Chem 20:4844–4852
13. Mei K, Kopp FK, Bippus R, Köhler T, Schwaiger BJ, Gersing AS, Fehringer A, Sauter A, Münzel D, Pfeiffer F, Rummeny EJ, Kirschke JS, Noël PB, Baum T (2017) Is multidetector CT-based bone mineral density and quantitative bone microstructure assessment at the spine still feasible using ultra-low tube current and sparse sampling? Eur Radiol 27:5261–5271
14. Yi JW, Park HJ, Lee SY, Rho MH, Hong HP, Choi YJ, Kim MS (2017) Radiation dose reduction in multidetector CT in fracture evaluation. Br J Radiol 90:20170240
15. Abbas S, Lee T, Shin S, Lee R, Cho S (2013) Effects of sparse sampling schemes on image quality in low-dose CT. Med Phys 40:111915
16. Beister M, Kolditz D, Kalender WA (2012) Iterative reconstruction methods in X-ray CT. Phys Med 28:94–108
17. Willemink MJ, de Jong PA, Leiner T, de Heer LM, Nievelstein RA, Budde RP, Schilham AM (2013) Iterative reconstruction techniques for computed tomography part 1: technical principles. Eur Radiol 23:1623–1631
18. Willemink MJ, Leiner T, de Jong PA, de Heer LM, Nievelstein RA, Schilham AM, Budde RP (2013) Iterative reconstruction techniques for computed tomography part 2: initial results in dose reduction and image quality. Eur Radiol 23:1632–1642
19. Noel PB, Fingerle AA, Renger B, Munzel D, Rummeny EJ, Dobritz M (2011) Initial performance characterization of a clinical noise-suppressing reconstruction algorithm for MDCT. AJR Am J Roentgenol 197:1404–1409
20. Noel PB, Renger B, Fiebich M, Munzel D, Fingerle AA, Rummeny EJ, Dobritz M (2013) Does iterative reconstruction lower CT radiation dose: evaluation of 15,000 examinations. PLoS One 8:e81141
21. Sidky EY, Kao CM, Pan X (2006) Accurate image reconstruction from few-views and limited-angle data in divergent-beam CT. J Xray Sci Technol 14:119–139
22. Zhao Z, Gang GJ, Siewerdsen JH (2014) Noise, sampling, and the number of projections in cone-beam CT with a flat-panel detector. Med Phys 41:061909
23. Zabic S, Wang Q, Morton T, Brown KM (2013) A low dose simulation tool for CT systems with energy integrating detectors. Med Phys 40:031102
24. Muenzel D, Koehler T, Brown K, Žabić S, Fingerle AA, Waldt S, Bendik E, Zahel T, Schneider A, Dobritz M, Rummeny EJ, Noël PB (2014) Validation of a low dose simulation technique for computed tomography images. PLoS One 9:e107843
25. Ramachandran GN, Lakshminarayanan AV (1971) Three-dimensional reconstruction from radiographs and electron micrographs: application of convolutions instead of Fourier transforms. Proc Natl Acad Sci U S A 68:2236–2240
26. Fessler JA (2000) Statistical image reconstruction methods for transmission tomography. In Fitzpatrick JM, Sonka M (eds) handbook of medical imaging, volume 2 medical image processing and analysis. SPIE publications, pp 1-70
27. Fehringer A, Lasser T, Zanette I, Noel PB, Pfeiffer F (2014) A versatile tomographic forward- and back-projection approach on multi-GPUs. Proc SPIE 9034, medical imaging 2014: image processing, 90344F (21 march 2014)

28. Kim D, Ramani S, Fessler JA (2015) Combining ordered subsets and momentum for accelerated X-ray CT image reconstruction. IEEE Trans Med Imaging 34:167–178
29. Lange K (1990) Convergence of EM image reconstruction algorithms with Gibbs smoothing. IEEE Trans Med Imaging 9:439–446
30. Huber PJ (1964) Robust estimation of a location parameter. Ann Math Statist 35:73–101
31. Schneider CA, Rasband WS, Eliceiri KW (2012) NIH image to ImageJ: 25 years of image analysis. Nat Methods 9:671–675
32. Schindelin J, Rueden CT, Hiner MC, Eliceiri KW (2015) The ImageJ ecosystem: an open platform for biomedical image analysis. Mol Reprod Dev 82:518–529
33. Fingerle AA, Noel PB (2018) Dose reduction in abdominal CT: the road to submillisievert imaging. Eur Radiol 28:2743–2744
34. Duan X, Wang J, Leng S, Schmidt B, Allmendinger T, Grant K, Flohr T, McCollough CH (2013) Electronic noise in CT detectors: impact on image noise and artifacts. AJR Am J Roentgenol 201: W626–W632
35. Yamamoto DS, Viale PH (2009) Update on identifying and managing osteoporosis in women with breast cancer. Clin J Oncol Nurs 13:E18–E29
36. Gralow JR, Biermann JS, Farooki A, et al. (2013) NCCN task force report: bone health in Cancer care. J Natl Compr Canc Netw 11 Suppl 3:S1-50; quiz S51
37. Gralow JR, Biermann JS, Farooki A, et al. (2009) NCCN task force report: bone health in Cancer care. J Natl Compr Canc Netw 7 Suppl 3:S1-32; quiz S33-35
38. Guise TA (2006) Bone loss and fracture risk associated with cancer therapy. Oncologist 11:1121–1131